Coalescence of low-viscosity fluids in air

Sarah C. Case
The James Franck Institute and Department of Physics, University of Chicago, Chicago, Illinois 60637, USA
(Received 7 September 2008; published 9 February 2009)

An electrical method is used to study the early stages of coalescence of two low-viscosity drops. A drop of aqueous NaCl solution is suspended in air above a second drop of the same solution, which is grown until the drops touch. At that point a rapidly widening bridge forms between them. By measuring the resistance and capacitance of the system during this coalescence event, one can obtain information about the time dependence of the characteristic bridge radius and its characteristic height. At early times, a new asymptotic regime is observed that is inconsistent with previous theoretical predictions. The measurements at several drop radii and approach velocities are consistent with a model in which the two liquids coalesce with a slightly deformed interface.

DOI: 10.1103/PhysRevE.79.026307 PACS number(s): 47.55.D−, 68.03.−g, 47.55.N−

I. INTRODUCTION

All around us we see fluid drops joining together: raindrops splash into a pond and fuse with it; individual drops falling from a faucet merge together to fill a glass of water. It is easy to forget the wonder of such a ubiquitous phenomenon. There is a change in topology when two fluids coalesce. As soon as they come into contact, a fluid bridge is formed between the two masses. The initial radius of the bridge is much smaller than the macroscopic dimensions of the flow. Interfacial tension then widens it until the two drops merge into a single entity. A video sequence of this process is shown in Fig. 1. Another common example of a topological transition is the inverse process to coalescence—that is, drop breakup [1–5]. There, a single mass of fluid separates into two segments joined by a thin neck. In that case the topological transformation proceeds as a physical dimension, the neck radius, and approaches zero, causing the dynamics to approach a singularity. When two drops coalesce, we expect similar singular behavior.

Such fluid transitions have often been compared to critical thermodynamic phase transitions, as this separation of length scales often leads to universal behavior [6–8]. Although it is an appealing and useful framework, it was recently discovered that not all fluid-breakup singularities obey universal dynamics [9,10]. In light of this, it is imperative to consider other familiar fluid transitions, such as drop coalescence, to see if they, too, behave in unexpected ways. Moreover, drop coalescence is of practical as well as purely scientific importance. Viscous sintering, emulsion stability, and mixing in microfluidics often need to be controlled in industrial processes. In this paper, I employ an electrical method to explore the drop coalescence transition at low viscosities at times three orders of magnitude earlier than previous optical experiments.

Coalescence processes occur in both the viscous regime, where the primary force opposing the widening of the bridge between the drops is due to viscous dissipation, and the inviscid regime, where the widening of the bridge is opposed primarily by inertial forces. In the inviscid regime studied here, the radius of the fluid bridge between the two coalescing drops, r, is much greater than the viscous length scale of the system, $l_\nu=\mu^2/\rho\gamma$, where μ is the dynamic viscosity of the fluid, ρ is its density, and γ is the surface tension. For water coalescing in air, $l_\nu\approx 14$ nm, and viscous effects can be neglected for much of the coalescence. This regime has been studied less than its high-viscosity counterpart [11,12] because the very rapid initial motion of the low-viscosity fluid is difficult to resolve in experiments and computations. However, theory has predictions.

A straightforward scaling argument [11] can be used to describe coalescence in the inviscid regime. To initiate coalescence, the drops must be brought very close together. Soon after the bridge is formed, the gap width between the two drops, d, will satisfy $d \ll r$. In this case, a balance between surface tension and inertia leads to

$$\left(\frac{\gamma}{\rho d}\right)^{1/2} \propto \frac{dr}{dt}. \tag{1}$$

It is assumed that if the two droplets are brought together sufficiently slowly, then they will maintain a spherical shape. For hemispherical drops, $d=r^2/A$, where A is the drop radius, as shown in Fig. 2. The resulting differential equation can be solved, where t_0 is the instant at which coalescence occurs and c is a proportionality constant of order unity:

$$r = c\left(\frac{4\gamma A}{\rho}\right)^{1/4}(t-t_0)^{1/2}. \tag{2}$$

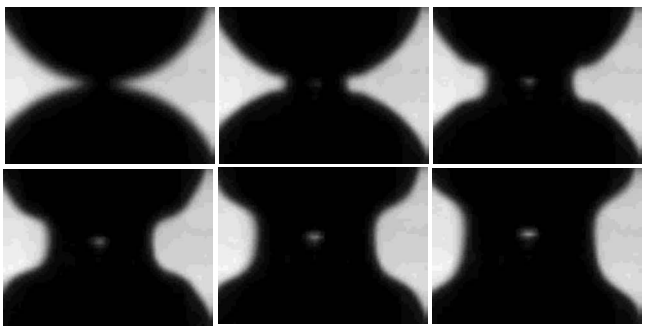

FIG. 1. Two drops of aqueous NaCl solution at saturation of radius $A=1$ mm are coalescing. The frames are 69 μs apart. The white spot in the bridge center is an optical artifact due to the drop lensing the light source located behind it.

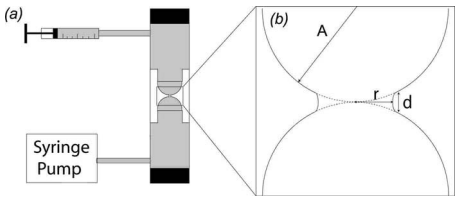

FIG. 2. (a) Experimental setup. Two acrylic tubes of length 5 cm long and inner diameter 0.95 cm are secured in line with one another. Changeable nozzles of radius A are attached to each tube. The nozzle tips are separated by $2A$. A drop of aqueous NaCl solution is formed on the upper nozzle using a microliter syringe, and the lower drop is then slowly grown until the two drops coalesce, using a variable-speed syringe pump (Kazel R99-FM) with syringe sizes varying from 50 μl to 20 ml and injection speeds varying from 0.21 to 70.0 ml/h. (b) Coalescence of two drops. Two drops of radius A meet at a single point. A bridge of radius r and height d forms and expands due to the interfacial tension γ. For hemispherical drops, $d \sim r^2/A$.

This scaling law has been supported by simulations studying the coalescence of low-viscosity fluid drops in the absence of an outer fluid [13,14]. However, due to the speed and the geometry of the transition, experimental studies have been unable to confirm the applicability of this scaling law to times $(t-t_0) \equiv \tau < 10$ μs.

Previous experiments have observed $r \propto (t-t_0)^{1/2}$ for $(t-t_0) > 10$ μs using high-speed imaging at rates up to 10^6 frames per second [15–17], as well as ultrafast x-ray phase-contrast imaging [18]. However, one aspect of the data suggests that the dynamics may not behave as we would expect. In one experiment, a small dc voltage was placed across the drops, and it was found that the initiation of electrical contact occurred 20–50 μs before coalescence could be observed visually [15]. An electrical method introduced by Case and Nagel [19], expands the measurement range down to $\tau \sim 10$ ns, a region currently inaccessible to imaging experiments. Results from these data closer to the instant of coalescence indicated a new asymptotic regime not predicted by the scaling argument given above. Moreover, it suggested a solution to the discrepancy found between the instant of electrical contact and the apparent initiation of coalescence.

Electrical methods for studying drop coalescence have been used in other experiments. The electrical method used in Case and Nagel's experiment is similar to one previously developed by Burton *et al.* [20], which used a small dc voltage to measure the resistance of a mercury droplet during breakup. Case and Nagel extended the technique of Burton *et al.* by using an ac voltage to measure separately both the time-dependent resistance and the capacitance of two coalescing drops of aqueous NaCl solution. This enabled them to infer the geometry of the coalescing region as early as 10 ns after the instant of coalescence. They found a new asymptotic regime at early times that is not consistent with the predictions of the simple scaling argument outlined above. This behavior occurs for $\tau < 10$ μs so that it is entirely in the region that cannot be studied by direct imaging. In addition, an ac electrical method was used by Lukyanets and Kavehpour to study the rest time of coalescing drops [21]. These results (at voltage magnitudes three orders of magnitude larger than the largest used here) suggest that deformations resulting from high electric fields in the gap between the two drops may introduce errors in measurements. In the experiments described here, varying the voltage and frequency by several orders of magnitude does not significantly affect the results. This is discussed further in Appendix A.

In this paper, I expand upon these measurements and provide a more detailed experimental description. I vary experimental parameters such as the drop diameter and approach velocity in order to explore further the surprising behavior seen in the initial experiments. My experiments support the hypothesized new asymptotic regime at the earliest times measured.

II. EXPERIMENTAL DESCRIPTION

A. Impedance measurement

In this experiment, two drops of aqueous sodium chloride solution at saturation coalesce in air at room temperature. At saturation, or 26% NaCl by mass, the fluid parameters of salt water are fluid density $\rho = 1.1972$ g/cm, kinematic viscosity $\nu = 1.662$ cS, surface tension $\gamma = 82.55$ dyn/cm, and conductivity $\sigma = 0.225$ $(\Omega\ \mathrm{cm})^{-1}$ [23].

As shown in Fig. 2, two acrylic tubes filled with salt water were aligned vertically. Teflon nozzles of radius A were attached to each tube, facing each other. Gold electrodes were immersed in salt water at the end of each tube opposite the nozzle. A known quantity of fluid was injected into each nozzle, forming two approximately hemispherical drops separated by a small distance. An ac voltage of frequency f and magnitude $|V|$ was applied across the electrodes, and the lower drop was then slowly grown at a fixed rate until the two drops coalesced. The complex impedance of the experimental cell, Z_{cell}, was measured as a function of time during the coalescence.

To evaluate Z_{cell}, we used the Wheatstone bridge arrangement shown in Fig. 3. A known impedance Z_t was connected in series with our measuring device, a National Instruments PCI-5105 simultaneous sampling digitizer. The effective input impedance of the PCI-5105, Z_0, is its stated input impedance R_0 in parallel with the cable capacitance C_0 of the coaxial cable. The experimental cell was also connected in series with the measuring device and in parallel with the combination of Z_t and Z_0. A Hewlett-Packard HP3325A function generator was connected in series with Z_t.

The voltage V_r was measured between Z_t and Z_0, and V_s was measured between Z_{cell} and Z_0. These voltages were sampled simultaneously at a maximum rate of 60 MHz. The sampling rate was $10f$, where f is the frequency of the input sine wave from the function generator, except for data taken at $f = 10$ MHz, which was sampled at the maximum rate of 60 MHz. The voltages were read into Labview (National Instruments) and analyzed. The analysis averaged the incoming signals over a single period to find the ratio of their amplitudes, $|V_r|/|V_s|$, as a function of time t. In addition, the analysis compared the input signals to a known sine wave and found the relative phase shift of each signal versus t. These

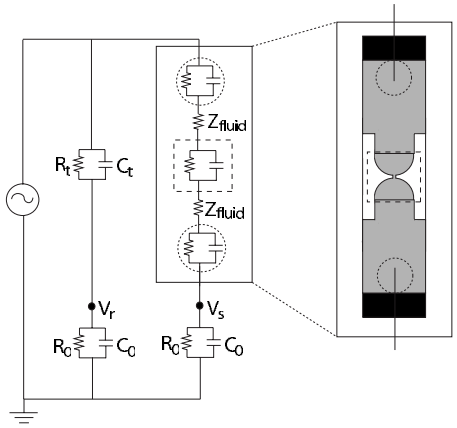

FIG. 3. Measurement circuit. Gold electrodes 0.5 mm in diameter and 1 cm long are secured in the measurement cell and connected to the circuit shown. The ac source is an HP 3325A function generator (Hewlett-Packard). The upper left branch consists of known circuit elements (R_t and C_t), while each lower branch is the input impedance of the oscilloscope (R_0) in parallel with the capacitance of the coaxial cables connecting the circuit to the oscilloscope (C_0). In place of a traditional oscilloscope we use an NI PCI-5105 high-speed simultaneous sampling digitizer. The impedance of the cell can be separated into three contributions, added in series: $Z_{electrodes}$, Z_{fluid}, and Z_{CR}. $Z_{electrode}$ can be modeled as a frequency-dependent capacitance due to the double layer, in parallel with an equivalent resistance due to charge transfer, as shown in the dotted circle [22]. The impedance of the coalescing region, Z_{CR}, can be modeled as a capacitor, due to the large exposed surface of the two drops, in parallel with a resistance, as shown in the dashed square.

phase shifts were subtracted to find $\Delta\phi$, the phase shift between V_r and V_s as a function of t.

Using the complex equation

$$\frac{|V_r|}{|V_s|}e^{-i\Delta\phi} = \frac{|Z_{cell} + Z_0|}{|Z_t + Z_0|}e^{-i\Delta\phi} \tag{3}$$

allowed Z_{cell} to be calculated as a function of the known circuit elements Z_t and Z_0 and the measured values of $|V_r|/|V_s|$ and $\Delta\phi$:

$$\mathrm{Re}(Z_{cell}) = \frac{2|Vr|}{|Vs|}\{[\mathrm{Re}(Z_0) + \mathrm{Re}(Z_t)]\cos\Delta\phi - [\mathrm{Im}(Z_0) + \mathrm{Im}(Z_t)]\sin\Delta\phi\} - \mathrm{Re}(Z_0),$$

$$\mathrm{Im}(Z_{cell}) = \frac{2|Vr|}{|Vs|}\{[\mathrm{Re}(Z_0) + \mathrm{Re}(Z_t)]\sin\Delta\phi + [\mathrm{Im}(Z_0) + \mathrm{Im}(Z_t)]\cos\Delta\phi\} - \mathrm{Im}(Z_0).$$

The circuit was calibrated by replacing Z_{cell} with known circuit elements, and the measured values of Re(Z) and Im(Z) were shown to be consistent across the frequency range with the values of the known circuit elements. Equation (3) assumes that the input impedance for the PCI-5105 is identical for both input channels. This is not necessarily the case, and the analysis allowed this to be varied in order to calibrate the cell. Within the known error of the input impedances, however, they were identical, and this equation is accurate.

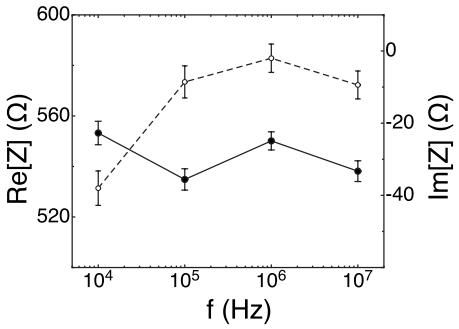

FIG. 4. Cell impedance. The real and imaginary parts of $Z_{closed}=Z_{electrodes}+Z_{fluid}$ are shown as functions of frequency. The open symbols show Im(Z_{closed}), and the solid symbols show Re(Z_{closed}).

B. Isolating the impedance of the coalescing region

The impedance of the experimental cell, Z_{cell}, has three distinct contributions, as shown in Fig. 3. It can be shown that for the voltage across the cell, $|V_{cell}| \lesssim 50$ mV, the interaction of the electrodes with the solution produces an effective contribution to the impedance that is equivalent to a resistor in parallel with a frequency-dependent capacitor [22]. We represent this contribution as $Z_{electrodes}$. Also, the "coalescing region" (defined as the region between the tips of the two nozzles) contributes an impedance Z_{CR}. Finally, the fluid between the electrodes and the coalescing region contributes an impedance Z_{fluid}. $Z_{electrodes}$ depends on the frequency f, while Z_{fluid} is independent of f. As these contributions are in series, we can write

$$Z_{cell} = Z_{electrodes} + Z_{fluid} + Z_{CR}. \tag{4}$$

If the two nozzle tips are brought into contact, $Z_{closed} = Z_{electrodes} + Z_{fluid}$. A representative measurement of Z_{closed} as a function of frequency is shown in Fig. 4 for $A = 1$ mm. This measurement allows Z_{CR} to be isolated from the other contributions in the cell:

$$Z_{CR} = Z_{cell} - Z_{closed}. \tag{5}$$

During coalescence, Z_{CR} can be considered as a resistor R_{CR}, representing the resistance of the two drops and the bridge between them, in parallel with a capacitance C_{CR}, representing the capacitance of the conducting surfaces. Both the resistance and the capacitance change with time and are related to the geometry of the coalescing region.

During the 10 μs before coalescence occurs, $Z_{CR} = -i/2\pi f C_{CR}$ represents the capacitance of the drop tips as well as the other conducting surfaces of the cell. We consider C_{init}, the capacitance of the two drops just before coalescence occurs, to be in parallel with the capacitance of the rest of the system, C_{cell}. This approximation is supported by electrostatic simulations (see Appendix B). Thus, in order to isolate C_{init}, we calculate $C_{init} = C_{CR} - C_{cell}$, where C_{cell} is the mea-

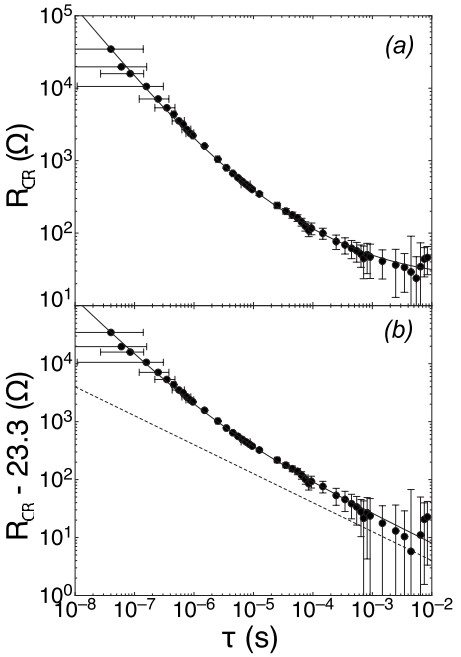

FIG. 5. Measured resistance during droplet coalescence. (a) R_{CR} versus $\tau=(t-t_0)$. The solid line shows $R_{CR}=1.2\times10^{-3}\tau^{-1}+0.8\tau^{-1/2}+23.3$. (b) $R_{CR}-23.3\ \Omega$ versus τ. The solid line shows $R_{CR}=1.2\times10^{-3}\tau^{-1}+0.8\tau^{-1/2}$. The dashed line shows $R_{CR}\sim\tau^{-1/2}$. In each case, $A=1$ mm, and the drops approach one another at a rate of 0.0004 A/ms. The data are an average of 24 individual coalescence events, 6 obtained at each of 4 measurement frequencies. The error bars reflect the spread in these measurements as well as systematic error due to inaccuracies in the measurement of $Z_{electrode}$ and due to the choice of t_0, the instant of coalescence. Error bars are shown both for τ and for R_{CR}.

sured capacitance of the cell when no drops have been formed on the nozzle tips. In our experiments, we measure both R_{CR} and C_{CR} as functions of time after the bridge is formed, as well as C_{init} before the bridge is formed.

III. RESULTS AND DISCUSSION

A. Resistance and capacitance during coalescence

The resistance of the coalescing region is shown versus $\tau\equiv t-t_0$ in Fig. 5(a) for $A=1$ mm. We determine the instant of coalescence (t_0) from the phase shift between $|V_r|$ and $|V_s|$ to within a period of the oscillation, $\pm1/f$. We adjust t_0 within this range such that the earliest data taken at a given frequency overlap the data taken at higher f. This is impossible for the highest-frequency data.

The data are well described by the form $R_{CR}=\alpha\tau^{-1}+\beta\tau^{-1/2}+\delta$. The best fit to the data, shown by the solid line, gives $\alpha=(1.2\pm0.3)\times10^{-3}$, $\beta=0.8\pm0.2$, and $\delta=23.3\pm15$. Figure 5(b) shows the same data as in Fig. 5(a), plotted as $R_{CR}-23.3\ \Omega$ versus τ. The dashed line shows a power law $\tau^{-1/2}$, while the solid line shows the same fit as in Fig. 5(a).

C_{init} versus τ is shown in the solid symbols in Fig. 6 and is constant within error. The solid line shows the average value of $C_{CR}=1.30\pm0.14$ pF. The open symbols show $C_{init}=C_{CR}-C_{cell}$ versus τ, where $C_{cell}=0.89\pm0.02$ pF. The average value $C_{CR}=0.41\pm0.14$ pF is shown by the dashed line. All capacitance measurements are obtained at 10 MHz, as at lower frequencies, $|V_s|$ is comparable to electrical noise.

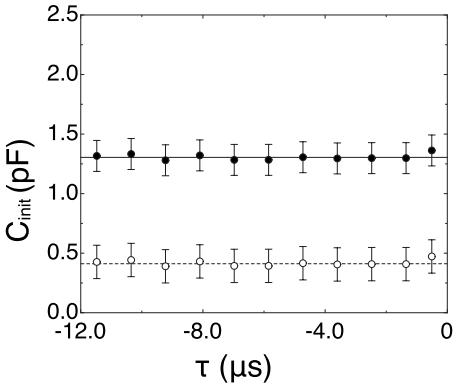

FIG. 6. Measured capacitance before droplet coalescence. The solid symbols show C_{CR} versus τ. The solid line shows $C_{CR}=1.3$ pF. The open symbols show $C_{init}=C_{CR}-C_{cell}$ pF. The dashed line shows $C_{init}=0.41$ pF. The data are an average of three individual coalescence events taken at $f=10$ MHz. The error bars reflect the spread in these measurements as well as systematic error.

B. High-speed imaging data

In addition to our electrical measurements, we verified previous measurements of the bridge radius during drop coalescence using a high-speed digital camera (Phantom v.7) running at 144 000 frames per second. Images are shown in Fig. 1. The resolution used was 26 μm/pixel, and we used simultaneous electrical measurements to determine t_0. A sample measurement of r versus τ for $A=1$ mm is shown in Fig. 7. The best fit to the data for $\tau<1$ ms gives $r=(3.2\pm0.5)\tau^{0.50\pm0.02}$ for $\tau>100\ \mu$s, which is consistent with previous measurements. This exponent is consistent with the scaling argument assuming $d\propto r^2$ summarized by Eq. (2), which predicts $r=2.3\tau^{1/2}$.

C. Comparison to predictions from scaling argument

We predict R_{CR} by considering the geometry of the coalescing region. R_{CR} can be separated into three pieces con-

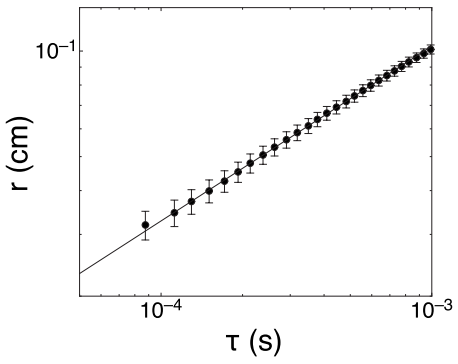

FIG. 7. High-speed imaging. r versus τ is shown for a representative coalescence event. The solid line shows $r=3.2\tau^{0.50}$. The frame rate is 144 000 frames per second.

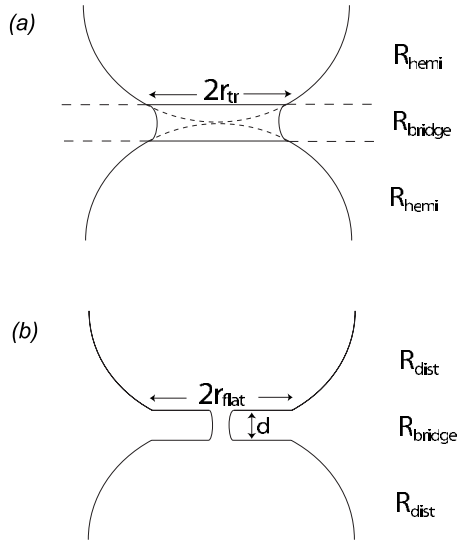

FIG. 8. Two geometries for coalescence. (a) Two hemispherical drops of radius A coalesce. We separate the resistance R_{CR} into three parts. R_{hemi} is the resistance of the hemispherical shapes, which are cut off as they come into contact with the bridge. R_{bridge} gives the resistance of the bridge with radius $r=r_{tr}$. (b) Two drops of radius A coalesce with flattened tips. The radius of the flattened region is given by r_{flat}. For $r<r_{flat}$, d=const, while for $r>r_{flat}$, $d=r^2/A$. The resistance of the flattened hemispheres is given by R_{dist}.

nected in series: $R_{CR}=R_{upper}+R_{bridge}+R_{lower}$. R_{upper} is the resistance of the upper drop, R_{lower} is the resistance of the lower drop, and R_{bridge} is the resistance of the bridge between the two drops.

We assume that both drops are hemispheres of radius A, and so $R_{upper}=R_{lower}\equiv R_{hemi}$. Therefore, we write $R_{CR}=2R_{hemi}+R_{bridge}$. Due to the vertical alignment of the nozzles, gravity can distort the drop shapes slightly. However, for length scales much smaller than the capillary length $l_c=\sqrt{\gamma/\rho g}$, the surface tension pressure maintaining a spherical shape is stronger than gravity. For the aqueous NaCl solution, $l_c=2.7$ mm, while our largest drops have $A=2$ mm.

We model R_{hemi} as a hemisphere truncated by a plane parallel to the flat surface of the hemisphere. The plane intersects the hemisphere with a radius of r_{tr}, as seen in Fig. 8(a). We numerically calculate the resistance of this shape using the electrostatics calculation package ESTAT (FieldCo), varying r_{tr} over several orders of magnitude. We find that $R_{hemi}=\frac{1}{4}r_{tr}\sigma$, where σ is the conductivity of the fluid.

R_{bridge} can be estimated directly. The resistance of a roughly cylindrical object scales as the length divided by the area, yielding $R_{bridge}\sim d/\sigma\pi r^2$. For two hemispherical drops, the gap width $d\sim r^2/A$, and therefore $R_{bridge}\sim(\sigma\pi A)^{-1}$, a constant. Using these results and the relation between r and τ from the scaling argument in Eq. (2), we find

$$R_{CR}=\frac{1}{2\sigma}\left(\frac{\rho}{4c\gamma A}\right)^{1/4}\tau^{-1/2}+\frac{1}{\sigma\pi A}. \tag{6}$$

This equation is calculated for the salt water and air system with $A=1$ mm and $R_{CR}=0.97\tau^{-1/2}+14$. For $\tau>10$ μs, this prediction is in qualitative agreement with our data, as can be seen in Fig. 5(b). However, for $\tau<10$ μs, our data show R_{CR} to be significantly larger than predicted. Thus the early-time data suggest a new asymptotic regime not included in the scaling prediction of Eq. (2).

We can estimate C_{init} in this geometry by modeling the system as two conducting hemispheres separated by a distance z. When $z\ll A$, the capacitance of this arrangement of conductors is comparable to that of a sphere of radius $A/2$ suspended with its tip a distance z above an infinite conducting plane, which can be solved analytically. An approximation for $z/A\ll 1$ [24] shows

$$C_{init}\approx\pi\epsilon_0 A\left[\ln\left(\frac{A}{2z}\right)+1.84\right]. \tag{7}$$

Due to the logarithmic dependence of C_{init} on z, uncertainty in the measurement of $C_{init}=0.41\pm0.14$ pF leads to enormous variation in the calculated value of z: from 190 nm for $C_{init}=0.27$ pF to 8.05×10^{-3} nm for $C_{init}=0.55$ pF.

D. Alternative interpretation: Flattened drop tips

To explain the discrepancy at small τ between the predictions of the model and the data, a modification to the coalescence geometry was proposed [19]. In deriving $r\propto\tau^{1/2}$, it was assumed that $d\propto r^2$. However, if the drop tips are slightly flattened, as in Fig. 8(b), a different dependence is found for $r(\tau)$ at early times.

For hemispherical drops with a flattened tip of radius r_{flat}, $d\propto r^2$ only when $r>r_{flat}$. For $r<r_{flat}$, d is constant, and the problem is equivalent to that of a hole opening in a thin film due to interfacial tension. As long as we remain in the inviscid regime, Eq. (1) still applies, and solving for d constant, we find

$$r=c'\left(\frac{\gamma}{\rho d}\right)^{1/2}\tau. \tag{8}$$

In this geometry, R_{CR} is calculated by replacing R_{hemi} for the undistorted case with R_{dist}, the resistance of the distorted hemisphere in Fig. 8(b) that has a flattened tip of radius r_{flat}. The flattened hemisphere has a small opening in its base of radius r which corresponds to the bridge. A numerical solution shows $R_{dist}=1/4r\sigma$. We estimate $R_{bridge}=d/\sigma\pi r^2$. Combining these contributions with the time dependence seen in Eq. (8) yields

$$R_{CR}=\frac{1}{2\sigma}\left(\frac{\rho}{\gamma}\right)^{1/2}\frac{d^{1/2}}{\tau}+\frac{\rho}{\sigma\pi\gamma}\frac{d^2}{\tau^2}. \tag{9}$$

Thus, when $r<r_{flat}$, R_{CR} is independent of A.

The predictions of this model can be compared to the data shown in Fig. 5(a). A transition time t_t from $\tau^{-1/2}$ behavior to τ^{-1} behavior is determined to be $0.87\ \mu s\leqslant t_t\leqslant 6.5\ \mu$s with the best fit being $t_t=2.4$ μs. For $t\ll t_t$, $R_{CR}\approx(1.2\times10^{-3}\pm3\times10^{-4})\tau^{-1}$. From the argument above, this prefactor is $(\rho d/\gamma)^{1/2}/2\sigma$. Comparing the prediction to the data yields $d=200\pm100$ nm.

The contribution from the τ^{-2} term is negligible. R_{CR} crosses over from τ^{-1} behavior to τ^{-2} behavior at a time t_c

$=(0.077\ \mathrm{s/cm^{-3/2}})d^{3/2}$. When $d=200\pm100$ nm, $t_c=7\pm5$ ns. This is beyond the measurement window; the experiments would only resolve $R_{CR}\propto d^{1/2}/\tau$ at the earliest times measured.

In this model, C_{init} is dominated by the flattened region. We approximate C_{init} as a parallel-plate capacitor of area πr_{flat}^2 and separation d. Using Eq. (2) and the crossover time t_t from $\tau^{-1/2}$ to τ^{-1} behavior gives $22\ \mu\mathrm{m}\leqslant r_{flat}\leqslant 59\ \mu\mathrm{m}$ with the best-fit value (from the best fit for t_t above) $r_{flat}\approx 36\ \mu$m. This approximation then yields a capacitance $0.04\ \mathrm{pF}\leqslant C\leqslant 0.97$ pF with the best fit $C=0.18$ pF. Using electrostatic simulations in combination with Eq. (7), I find that the hemispherical region contributes approximately 0.07 pF to the capacitance. Assuming these parallel contributions can be added, I find that $0.11\ \mathrm{pF}\leqslant C_{CR}\leqslant 1.04$ pF, which is consistent with the measurement $C_{init}=0.41$ pF.

E. Varying the drop radius A

The model with the flattened tips has two regimes. Equation (9) should hold for $t\ll t_c$, where t_c represents the time at which R_{CR} crosses over from τ^{-1} to τ^{-2} behavior. At longer times, $t\gg t_c$, R_{CR}, Eq. (6) should apply. Varying the drop radius A should only affect data for $t\gg t_c$.

I have measured R_{CR} for $A=2$ mm and $A=0.75$ mm in addition to the $A=1$ mm measurements already shown. For a drop with a flat tip, we expect that for $t\gg t_t$, $R_{CR}\approx 0.8\tau^{-1/2}+7$ for $A=2$ mm and $R_{CR}\approx 1.0\tau^{-1/2}+19$ for $A=0.75$ mm. At early times, we expect no change outside of error from the $A=1$ mm data for both drops.

The measured R_{CR} versus τ for $A=2$ mm and $A=0.75$ mm is shown in Fig. 9(a). For $A=2$ mm (open symbols), the best fit to the data is the dashed line: $R_{CR}=(1.2\pm0.3)\times10^{-3}\tau^{-1}+(0.7\pm0.2)\tau^{-0.50}+(10\pm10)$. For $A=0.75$ mm (solid symbols), the best fit is the solid line: $R_{CR}=(1.4\pm0.3)\times10^{-3}\tau^{-1}+(0.9\pm0.2)\tau^{-0.50}+(40\pm15)$. Our measurements thus give prefactors that are qualitatively consistent with those predicted by the flattened tip model.

C_{init} versus τ is shown for $A=2$ mm and $A=0.75$ mm in Fig. 9(b). C_{cell} for $A=2$ mm is measured to be 0.92 pF, and C_{cell} for $A=0.75$ mm is 0.81 pF. The measured capacitance for $A=0.75$ mm (shown as solid symbols) is larger than that seen for $A=1$ mm, and the average value before coalescence is $C_{init}-0.84=0.73\pm0.2$ pF (shown by the solid line.) For $A=2$ mm, we observe $C_{init}-0.92=0.52\pm0.14$ pF, which is within error of the value observed for $A=1$ mm.

In summary, when A is varied, we observe behavior which is consistent with the coalescence of two slightly flattened drops. For $\tau<1\ \mu$s, no difference is observed in R_{CR} when A is increased by a factor of 2.7. For $\tau\gg1\ \mu$s, the observations are consistent with the prediction that R_{CR} should increase for smaller drops. In the capacitance measurements, we observe increases over the 1 mm measurement for both $A=0.75$ mm and $A=2$ mm. An increase in deformability could account for the increase observed for $A=2$ mm. For $A=0.75$ mm, we are unable to reach the low approach velocities used for larger drops, which may be responsible for the large capacitance observed.

F. Varying the drop velocity

The drops are brought together at a non-negligible approach velocity v. As v is increased, air effects will become more marked, particularly for larger drops, and may change the drop shape. We isolate such effects by varying the approach velocity. To account for the effects of different A, our units of velocity are A/ms.

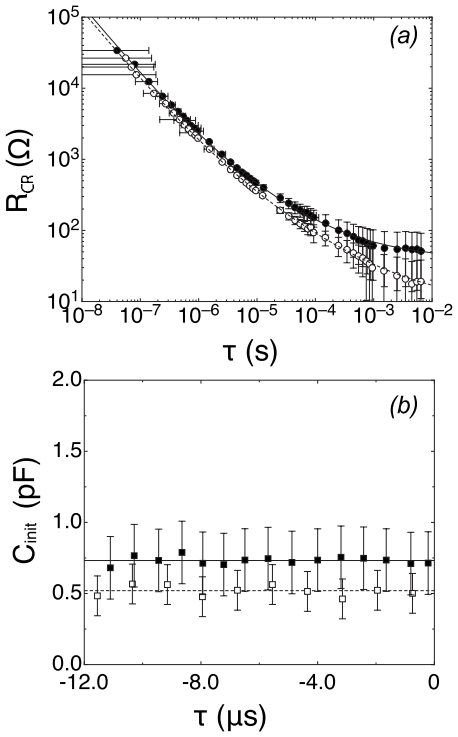

FIG. 9. Varying drop radius. The open symbols show $A=2$ mm. The solid symbols show $A=0.75$ mm. (a) R_{CR} versus τ. Data shown are the average of 12 individual coalescence events for each A. Three coalescence events were measured with each of four different f, from $f=10$ kHz to 10 MHz. The solid line shows $R_{CR}=1.4\times10^{-3}\tau^{-1}+0.9\tau^{-0.50}+40$. The dashed line shows $R_{CR}=1.2\times10^{-3}\tau^{-1}+0.7\tau^{-0.50}+10$. (b) C_{init} versus τ. Data shown are the average of three coalescence events taken at $f=10$ MHz. The dashed line shows $C_{init}=0.52$ pF. The solid line shows $C_{init}=0.73$ pF.

We show R_{CR} versus τ in Fig. 10(a), where the approach velocity is varied by a factor of 5 for $A=1$ mm. The solid symbols represent $v=0.0004\ A$/ms, while the open symbols represent $v=0.002\ A$/ms. Varying the velocity by this amount does not appreciably change the average data.

Figure 10(b) shows R_{CR} versus τ for $A=2$ mm, where the approach velocity is varied by a factor of 17. In this case, the solid symbols represent $v=0.0001\ A$/ms, and the open symbols represent $v=0.0017\ A$s/ms. The data for $v=0.0004\ A$/ms, shown previously, are within error of the $v=0.0001\ A$/ms data.

Figure 11 shows C_{init} versus τ for $v=0.0001\ A$/ms, $v=0.0004\ A$/ms, and $v=0.0017\ A$/ms, where $A=2$ mm. Three independent coalescence events are shown for each velocity. For $v=0.0001\ A$/ms and $v=0.0004\ A$/ms, the capacitance is very reproducible and $C_{init}=0.52\pm0.14$ pF. However, at $v=0.0017\ A$/ms, the capacitance is significantly larger and also less reproducible between different events.

We do not see a significant change in the data when we increase the approach velocity up to $v=0.002\ A$/ms for $A=1$ mm and up to $v=0.0004\ A$/ms for $A=2$ mm. The behav-

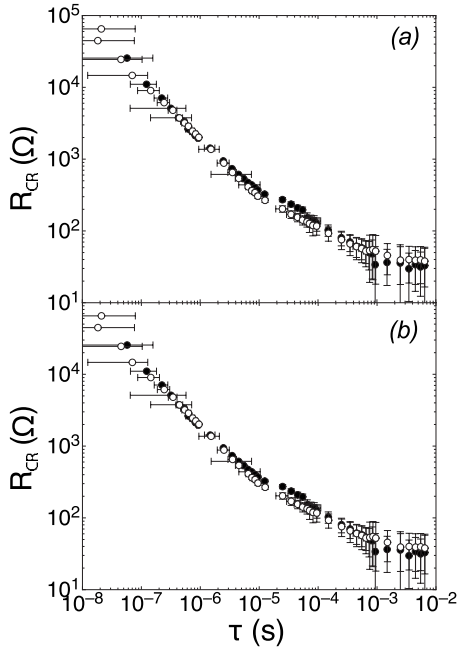

FIG. 10. Varying approach velocity. (a) R_{CR} versus τ for $A=1$ mm. The solid symbols show $v=0.0004$ A/ms. The open symbols show $v=0.0020$ A/ms. Data shown are the average of 12 individual coalescence events for each v. Three coalescence events occurred at each of four different f, from $f=10$ kHz to 10 MHz. (b) R_{CR} versus τ for $A=2$ mm. The solid symbols show $v=0.0001$ A/ms. The open symbols show $v=0.0017$ A/ms.

ior we see for drops $A=2$ mm, $v=0.0017$ A/ms is consistent with increased deformation of the drops. A highly deformed drop would coalesce at the same d as a less deformed drop, but t_c would occur later and the effective A could be expected to be larger. This leads to a lower R_{CR} than a hemispherical drop for $r > r_{flat}$, which we see for $A=2$ mm and $v=0.0017$ A/ms when compared to $v=0.0001$ A/ms. A large deformation would also increase C_{init} significantly, which we also observe in the highest-velocity data for $A=2$ mm. The

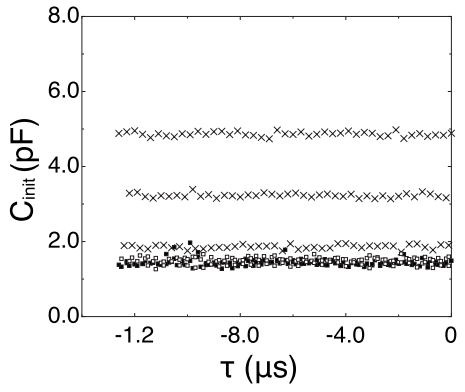

FIG. 11. Varying approach velocity. C_{init} versus τ. Solid symbols show data from three separate coalescence events for $v=0.0004$ A/ms. Open symbols show data from three separate coalescence events for $v=0.0001$ A/ms. The crosses show data from three separate coalescence events for $v=0.0017$ A/ms. All data shown were measured at $f=10$ MHz.

lack of reproducibility of C_{init} for $v=0.0017$ A/ms may indicate that the radius of the flattening is not consistent between different events at large velocity.

IV. CONCLUSIONS

In conclusion, an electrical method has been used to study the coalescence of two salt water drops. This method allows us to observe an unexpected asymptotic regime which becomes visible at $\tau < 10$ μs. Our data are consistent with the coalescence of two slightly flattened hemispherical drops. This is contrary to previous expectations, in which the drops were expected to maintain shapes described by quadratic minima. In addition, when A is varied by nearly a factor of 3, we continue to observe behavior which is consistent with the coalescence of two slightly flattened drops. Within error, we do not see a significant change in the data when we increase the approach velocity.

A previous theoretical description [13] has suggested that coalescence may occur as capillary waves cause repeated connections of the gap between the two drops. Each connection would entrain a toroidal bubble of the outer fluid. We see no evidence of this behavior in these experiments, which would appear as discrete jumps in R_{CR} during coalescence, as the neck width widens at each connection. It is possible that this behavior occurs on a time scale that is faster than the experiments described here are able to resolve.

Previous experiments using high-speed imaging have been unable to resolve this early-time regime. Additionally, they found that electrical contact occurred 20–80 μs before the first motions of coalescence were observed visually [15,16]. If the drops are coalescing in a flat region with $d \sim 100$ nm, it would be impossible to observe this stage of coalescence visually. It would only be possible to observe coalescence when d increased, entering into the hemispherical regime. We find that this occurs between 1 and 10 μs after the initiation of coalescence, consistent with these observations. These previous experiments also postulated that coalescence occurred over a finite region of radius ~ 100 μm. In this case, R_{CR} would increase suddenly at the instant of coalescence, contrary to our observations.

There are several possible reasons for the existence of a flattened region, and I suggest two here. One possibility is that the flattening is an air effect. It has recently been shown that for drops splashing on dry surfaces, air plays a role in the dynamics of the impact [25]. Two drops approaching one another at finite velocity might trap a layer of air between them, which could have unexpected consequences. A second possibility is the presence of surfactant. Although precautions were taken to avoid contamination,[1] surfactants might still be present in small quantities. It has been seen that even a very small amount of surfactant can prevent a drop from coalescing with a flat fluid surface [26]. The repulsion due to this could explain the observed flattening.

Understanding the flattening of two fluid drops as they approach each other could not only affect the many industrial

[1]Fresh fluid was used before each data set was taken. Also, the experiment was cleaned before each day of data taking.

applications that rely on droplet coalescence, but also could illuminate other important physical questions. The origin of the thin-film rupture which triggers coalescence is an active field of research [27]. The observable flattening of the drops could contribute to an understanding of this rupture. Also, as we begin to study the topological changes that occur in microfluidics, behavior at the smallest scales and the earliest times is essential.

The earliest stages of a topological transition in a fluid are when the analogy to a critical thermodynamic phase transition ought to be most accurate. As in drop breakup, near the coalescence transition, the small-scale flows decouple from the large-scale flows. However, we observe that the bridge radius between the two drops scales differently depending on the overall drop shape. The geometry of the system is crucial, a situation that does not have an analog in thermodynamic phase transitions. By studying these fluid shape transitions, we widen our understanding of the many unexpected ways in which nature produces these remarkable transformations.

ACKNOWLEDGMENTS

I am grateful to S. R. Nagel, L. N. Zou, X. Cheng, J. L. Wyman, N. Keim, E. Corwin, and J. Royer for helpful discussions and feedback. This research was supported by NSF MRSEC Grant No. DMR-0213745 and NSF Grant No. DMR-0652269.

APPENDIX A: CHECKS ON METHOD

Our experimental method, although similar to previous methods, has many novel elements. We present here several checks that we have performed to validate our data. This includes isolating electrical effects as well as using our method to study a better-understood topological change: that of drop snap-off of water in air.

1. Varying electrical parameters

a. Varying voltage magnitude

We begin by verifying that our measurements do not change if the magnitude of the ac voltage across the cell is changed. For $|V| \gtrsim 50$ mV, we cannot approximate the electrodes as a resistor in parallel with a capacitor, as the charge-transfer reaction no longer gives us $I \sim V$. In addition, large $|V|$ could deform the shape of the drops by increasing the attraction or repulsion between the surfaces.

During coalescence, as Z_{cell} changes, the voltage across the cell, V_{cell}, also changes in magnitude. We can determine a maximum $|V_{cell}|$, $|V_{max}|$ by assuming that the full voltage drop supplied by the function generator occurs across the experimental cell. We vary $|V_{max}|$ from 12.5 mV to 500 mV and find no significant difference in our data, as shown in Fig. 12(a) for three samples $|V_{max}|$. The noise becomes comparable to our signal at 12.5 mV, and all data used in the analysis are taken at $|V_{max}| = 50$ mV.

Additionally, as shown in the inset to Fig. 12(a), we examine the effect of varying $|V_{max}|$ from 50 mV to 500 mV on the measurement of C_{init} using measurement frequencies from $f = 6$ MHz to 15 MHz. No difference is seen outside of error.

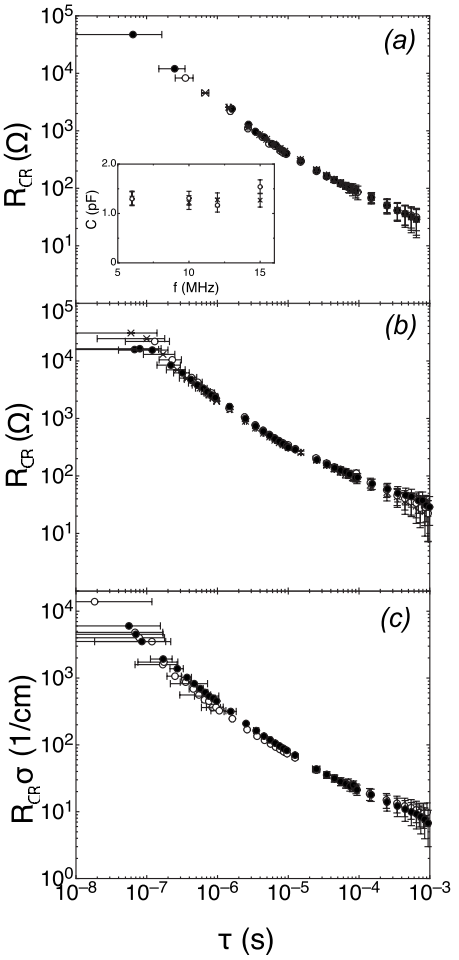

FIG. 12. Varying electrical parameters in resistance measurements. Each set of data shown is the average of 12 individual coalescence events. (a) Varying $|V_{max}|$. R_{CR} versus τ is shown. Solid symbols show $|V_{max}| = 25$ mV. Open symbols show $|V_{max}| = 50$ mV. Crosses show $|V_{max}| = 250$ mV. Inset shows C_{init} versus τ. Open symbols show $|V_max| = 50$ mV. Crosses show $|V_{max}| = 250$ mV. (b) Varying dc component. R_{CR} versus τ is shown. Solid symbols show no added dc component. Open symbols show an added dc component of 140 mV. Crosses show an added dc component of 35 mV. (c) Varying ionic concentration. R_{CR}/ρ_r versus τ is shown. Solid symbols show a 26% by mass solution (saturation), $\sigma = 0.2251/\Omega$ cm. Open symbols show a 10% by mass solution, $\sigma = 0.1261/\Omega$ cm.

b. Varying dc component of input signal

In addition to the ac signal applied across the experimental cell, a small amount of dc signal is observed. Any dc signal applied across the experimental cell before coalescence will polarize the cell, effectively charging it up like a capacitor. At the instant of coalescence, this capacitor discharges and a dc spike is observed. This spike has a typical maximum size $\sim 1-10$ μV, which is less than 1% of the typical output signal. We average the signal and remove this

dc contribution before analysis. We check the validity of this by explicitly adding up to 140 mV of dc to our signal. This did not alter our measurement within error, as can be seen in Fig. 12(b).

c. Varying ionic concentration

All data presented in the main body of the paper were taken with NaCl in water at saturation, or 26% by mass. We took the same set of measurements with solution of NaCl 15% by mass and 10% by mass. The conductivity σ changes by a factor of 2 between the NaCl solution at saturation and that at 10% by mass. All resistances measured should be inversely proportional to σ, and so to compare the different solutions we looked at $R_{CR}\sigma$. $R_{CR}\sigma$ versus τ is plotted in Fig. 12(c) and does not change, within error, as the concentration is varied.

With changing concentration, the fluid parameters also change slightly. For a solution of 10% NaCl by mass, $\rho = 1.0707\ \mathrm{g/cm^3}$, $\nu = 1.115$ cS, and $\gamma = 76.05$ dyn/cm. Calculating the predicted prefactors for the model, we find that the differences due to the fluid parameters are minimal, and we should not see effects from them outside of our experimental error.

2. Drop snap-off

Finally, we used our method to study drop breakup. We compare the output of our method against previous work, as well as our own calculations and find that they are consistent.

It has been previously observed that during drop snap-off, the neck between the two drops forms a self-similar cone with an angle of approximately 18°. We numerically calculated the resistance of a truncated cone of fixed larger radius as a function of the smaller radius r_{neck} and found $R_{CR} = 1.18/\sigma r_{neck}$ where σ is in units of $1/\Omega$ cm.

We used a Phantom V.7 fast digital camera at 144 000 frames per second to measure r_{neck} as a function of $t - t_0 = \tau$, where t_0 is the instant of snap-off. As shown in Fig. 13(a), the best fit to our data with $\tau < 1$ ms yields $r_{neck} = (1.2 \pm 0.6)\tau^{-0.66 \pm 0.06}$, which is in agreement with previous measurements of drop breakup of water in air.

As shown in Fig. 13(b), R_{CR} versus τ for a snap-off event yields a best fit of $R_{CR} = (5.7 \pm 0.9)\tau^{-0.67 \pm 0.01}$. This is shown as the dashed line in the figure. Combining the electrostatic calculation with the measured dependence of r_{neck} on τ, we predict that $R_{CR} = (5.24 \pm 2.63)\tau^{-0.66 \pm 0.06}$, within error of the data.

This indicates that the scaling law for breakup of water in air persists to time scales of 10 ns. Using the relation above, we calculate r_{neck} from R_{CR}. r_{neck} versus τ is shown in Fig. 13(c). The solid line is the best fit to the data, $r_{neck} = (0.75 \pm 0.01)\tau^{-0.67 \pm 0.01}$.

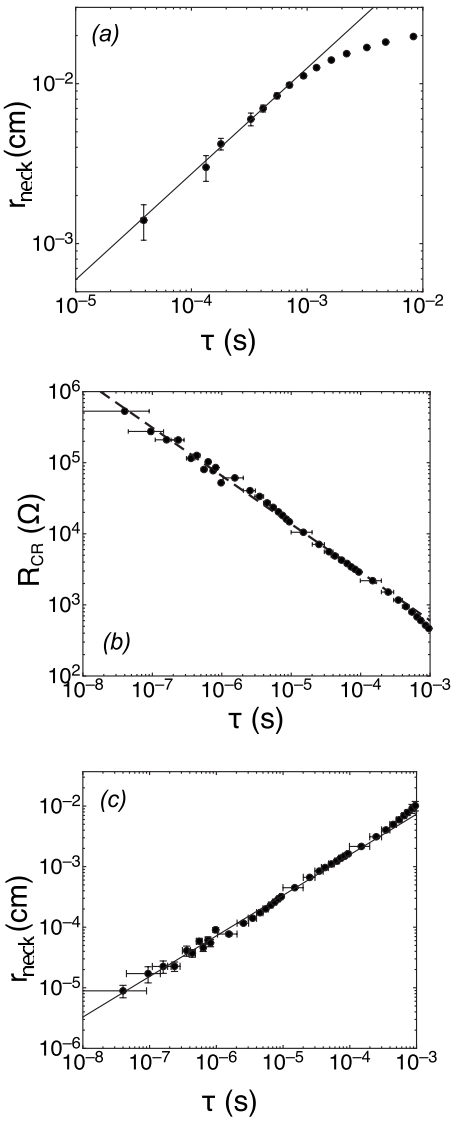

FIG. 13. Drop snap-off. (a) r_{neck} versus τ. r_{neck} was measured using high-speed imaging at 144 000 frames per second. The solid line shows $r = 1.2\tau^{-0.66}$ (b) R_{CR} versus τ. The dashed line shows $R_{CR} = 5.7\tau^{-0.67}$ (c) r_{neck} versus τ. r_{neck} calculated from electrical measurement of R_{CR}. The solid line shows $r_{neck} = 0.75\tau^{-0.67}$.

APPENDIX B: CAPACITANCE MEASUREMENTS

Before the bridge is formed, we need to separate the capacitance of the coalescing region, C_{CR} from the capacitance of the total arrangement of conductors. As stated in the experimental section, in order to achieve this, I measure the capacitance of the cell before any drops are formed on the nozzle tips, C_{cell}, and subtract this from the C_{CR} measured in the last μs before coalescence occurs.

I justify this approximation by simulating the axially symmetric part of the cell, including the nozzles and the tubes filled with NaCl solution. I find that for a fixed separation of the two drops ($A = 1$ mm) of $d = 1.5$ mm, $C_{CR} = 0.45$ pF from the simulation. Simulating the cell with no drops formed gives $C_{cell} = 0.44$ pF.

For a 1.5-mm separation between the drop tips, the measurements show $C_{CR} = 0.66 \pm 0.02$ pF and $C_{cell} = 0.62 \pm 0.02$ pF. When there is no fluid in the cell, we measure a stray capacitance of 0.2 pF, which accounts for the difference between the measurement and simulation if it can be considered to be in parallel with C_{CR}.

The capacitance of the cell outside the "coalescing region" is in parallel with C_{init}: thus, I estimate that C_{init}

$=C_{CR}-C_{cell}$. The simulation when $d=1.5$ mm yields $C_{CR}-C_{cell}=0.01$ pF, which is consistent with our measurement of $C_{CR}-C_{cell}=0.04\pm0.03$ pF.

In order to find C_{init} just before coalescence, I measure C_{cell} at the nozzle separation used for the coalescence measurements and subtract this from C_{CR}. For $A=1$ mm and a nozzle separation of 2 mm, $C_{cell}=0.89$ pF. The simulation predicts $C_{cell}=0.64$ pF in this case. This measurement is repeated for $A=2$ mm and $d=4$ mm, where $C_{cell}=0.92$ pF, and at $A=0.75$ mm and $d=1.5$ mm, where $C_{cell}=0.81$ pF.

[1] X. D. Shi, M. P. Brenner, and S. R. Nagel, Science **265**, 219 (1994).

[2] J. Eggers, Rev. Mod. Phys. **69**, 865 (1997).

[3] J. R. Lister and H. A. Stone, Phys. Fluids **10**, 2758 (1998).

[4] I. Cohen and S. R. Nagel, Phys. Fluids **13**, 3533 (2001).

[5] A. U. Chen, P. K. Notz, and O. A. Basaran, Phys. Rev. Lett. **88**, 174501 (2002).

[6] P. Constantin, T. F. Dupont, R. E. Goldstein, L. P. Kadanoff, M. J. Shelley, and S. M. Zhou, Phys. Rev. E **47**, 4169 (1993).

[7] R. E. Goldstein, A. I. Pesci, and M. J. Shelley, Phys. Rev. Lett. **70**, 3043 (1993).

[8] A. L. Bertozzi, M. P. Brenner, T. F. Dupont, and L. P. Kadanoff, in *Trends and Perspectives in Applied Mathematics*, edited by L. Sirovich (Springer, New York, 1996).

[9] P. Doshi, I. Cohen, W. W. Zhang, M. Siegel, P. Howell, O. Basaran, and S. R. Nagel, Science **302**, 1185 (2003).

[10] N. C. Keim, P. Moller, W. W. Zhang, and S. R. Nagel, Phys. Rev. Lett. **97**, 144503 (2006).

[11] J. Eggers, J. R. Lister, and H. A. Stone, J. Fluid Mech. **401**, 293 (1999).

[12] W. Yao, H. J. Maris, P. Pennington, and G. M. Seidel, Phys. Rev. E **71**, 016309 (2005).

[13] L. Duchemin, J. Eggers, and C. Josserand, J. Fluid Mech. **487**, 167 (2003).

[14] T. Lee and P. F. Fischer, Phys. Rev. E **74**, 046709 (2006).

[15] S. T. Thoroddsen, K. Takahara, and T. G. Etoh, J. Fluid Mech. **527**, 85 (2005).

[16] A. Menchaca-Rocha, A. Martínez-Dávalos, R. Núñez, S. Popinet, and S. Zaleski, Phys. Rev. E **63**, 046309 (2001).

[17] M. Wu, T. Cubaud, and C.-M. Ho, Phys. Fluids **16**, L51 (2004).

[18] K. Fezzaa and Y. Wang. (unpublished).

[19] S. C. Case and S. R. Nagel, Phys. Rev. Lett. **100**, 084503 (2008).

[20] J. C. Burton, J. E. Rutledge, and P. Taborek, Phys. Rev. Lett. **92**, 244505 (2004).

[21] A. Lukyanets and H. Kavehpour. (unpublished).

[22] J. O'M. Bockris, A. K. N. Reddy, and M. Gamboa-Aldeco, *Modern Electrochemistry*, 2nd ed. (Kluwer Academic, New York, 2000), Vol. 2A, pp. 1035–1166.

[23] *Handbook of Chemistry and Physics*, 58th ed. (CRC Press, West Palm Beach, 1977).

[24] L. Boyer, F. Houzé, A. Tonck, J.-L. Loubet, and J.-M. Georges, J. Phys. D **27**, 1504 (1994).

[25] L. Xu, W. W. Zhang, and S. R. Nagel, Phys. Rev. Lett. **94**, 184505 (2005).

[26] Y. Amarouchene, G. Cristobal, and H. Kellay, Phys. Rev. Lett. **87**, 206104 (2001).

[27] A. Oron, S. H. Davis, and S. G. Bankoff, Rev. Mod. Phys. **69**, 931 (1997).